JOINT INSTITUTE FOR NUCLEAR RESEARCH
Dzhelepov Laboratory of Nuclear Problems

FINAL REPORT ON THE START PROGRAMME

Study of ^{8}He/^{9}Li background in JUNO experiment

Supervisor:

Artem Vladislavovich Chukanov

Student:

Novikov Stepan, Moscow

Moscow State University

Participation period:

July 6 - August 23,

Summer Session 2025

Dubna 2025

Abstract

This paper presents a study of ^{8}He and ^{9}Li cosmogenic background isotopes in the Jiangmen Underground Neutrino Observatory (JUNO) experiment. These isotopes, produced by cosmic muon interactions with the liquid scintillator, represent one of the most challenging backgrounds for reactor antineutrino detection due to their decay signatures that mimic inverse beta decay events.

Contents

1 Introduction

1.1 The JUNO experiment and its physics goals

The Jiangmen Underground Neutrino Observatory (JUNO), situated in Kaiping, Guangdong Province, China (22.12°N, 112.52°E), is a state-of-the-art neutrino experiment designed as a 20-kiloton liquid scintillator detector located 700 meters underground to address fundamental questions in particle physics. The primary scientific objective of JUNO is the determination of the neutrino mass ordering (NMO), one of the fundamental unknowns in neutrino physics. The experiment is located approximately 1800 m water equivalent underground to minimize cosmic muon flux, which is reduced to 0.003 Hz/m². JUNO's ambitious scientific program aims to resolve the neutrino mass hierarchy with a significance of 3–4 σ after six years of data-taking. With six years of data, the neutrino oscillation parameters $\sin^2(\theta_{12})$, Δm^2_{21}, and $|\Delta m^2_{32}|$ can be measured to a precision of 0.6 or better, by detecting reactor antineutrinos from the Taishan and Yangjiang nuclear power plants.

Figure 1: JUNO location

Neutrinos, fundamental particles in the Standard Model, exhibit oscillations — a quantum mechanical phenomenon where they transition between electron (ν_e), muon (ν_μ), and tau (ν_τ) flavors—indicating non-zero masses and mixing. The Pontecorvo-Maki-Nakagawa-Sakata (PMNS) matrix governs these oscillations, parameterized by three mixing angles ($\theta_{12}, \theta_{13}, \theta_{23}$), a CP-violating phase (δ_{CP}), and two mass-squared differences (Δm^2_{21}, Δm^2_{31} or Δm^2_{32}). Current global fits yield $\Delta m^2_{21} \approx 7.53 \times 10^{-5}\,\mathrm{eV}^2$, $|\Delta m^2_{31}| \approx 2.52 \times 10^{-3}\,\mathrm{eV}^2$, $\sin^2\theta_{12} \approx 0.307$, $\sin^2\theta_{13} \approx 0.0218$, $\sin^2\theta_{23} \approx 0.536$, but the sign of Δm^2_{31} remains unresolved. This leads to two possible orderings: NO: $m_1 < m_2 < m_3$, IO: $m_3 < m_1 < m_2$

Additional physics goals include detecting $\sim 10^4$ solar neutrinos (^{7}Be, ^{8}B) annually, $\sim 10^3$ geoneutrinos over six years, and potential supernova neutrinos from a galactic burst at 10 kpc (expected ~ 5000 IBD events for a 10 $M_\odot$ progenitor). JUNO's interdisciplinary impact spans particle physics, astrophysics, and cosmology, potentially constraining models of leptogenesis, the matter-antimatter asymmetry, and neutrino interactions in dense astrophysical environments.

1.2 JUNO's detection strategy

Located at an optimal baseline of approximately 53 km from both the Yangjiang and Taishan Nuclear Power Plants (total thermal power of $26.6\,\mathrm{GW_{th}}$), JUNO is uniquely positioned to observe the subtle oscillation patterns that encode the neutrino mass hierarchy information (Fig.2). JUNO aims to determine this hierarchy by analyzing the interference patterns in the survival probability of reactor antineutrinos ($\bar{\nu}_e$), which are produced via β-decay in nuclear reactors.

The reactor antineutrino survival probability in vacuum can be written as

$$\begin{aligned} P(\bar{\nu}_e \to \bar{\nu}_e) \approx 1 & \\ & - \sin^2 2\theta_{13} \sin^2\left(\frac{\Delta m^2_{31} L}{4E}\right) \\ & - \sin^2 2\theta_{12} \sin^2\left(\frac{\Delta m^2_{21} L}{4E}\right), \end{aligned}$$

where L is the baseline ($\sim 53\,\mathrm{km}$) and E is the neutrino energy (~ 1–$10\,\mathrm{MeV}$). JUNO's sensitivity to the mass ordering arises from the interference between oscillation modes driven by Δm^2_{31} and Δm^2_{32}, making precise spectral measurements crucial for distinguishing between normal and inverted mass orderings.

1.3 Neutrino detection mechanism

The detection of antineutrinos in JUNO relies on the IBD reaction:

$$\bar{\nu}_e + p \to e^+ + n$$

Here, an electron antineutrino ($\bar{\nu}_e$) interacts with a free proton (p) in the liquid scintillator (LS) target, producing a positron (e^+) and a neutron (n). This reaction has an energy threshold of approximately 1.806 MeV, set by the neutron-proton mass difference (1.293 MeV) plus the positron rest mass (0.511 MeV).

Reactor antineutrinos, produced via beta decay in nuclear fission processes at nearby power plants (e.g., Yangjiang and Taishan, $\sim 53\,\mathrm{km}$ away with a total thermal power of $26.6\,\mathrm{GW_{th}}$), have energies typically ranging from ~ 1 to 10 MeV, making IBD an efficient detection channel.

JUNO expects an IBD event rate of approximately 60 events per day within its fiducial volume after selection cuts, based on the reactor antineutrino flux of $\sim 10^{20}\,\bar{\nu}_e$ per $\mathrm{GW_{th}}$ per year and the detector's 20-kilotonne LS target mass.

The positron produced in the IBD reaction travels a short distance ($\sim$cm) in the LS before losing its kinetic energy through ionization and bremsstrahlung, then annihilates with an ambient electron to produce two back-to-back 0.511 MeV gamma rays:

$$e^+ + e^- \to 2\gamma \quad (E_\gamma = 0.511\,\mathrm{MeV\ each}).$$

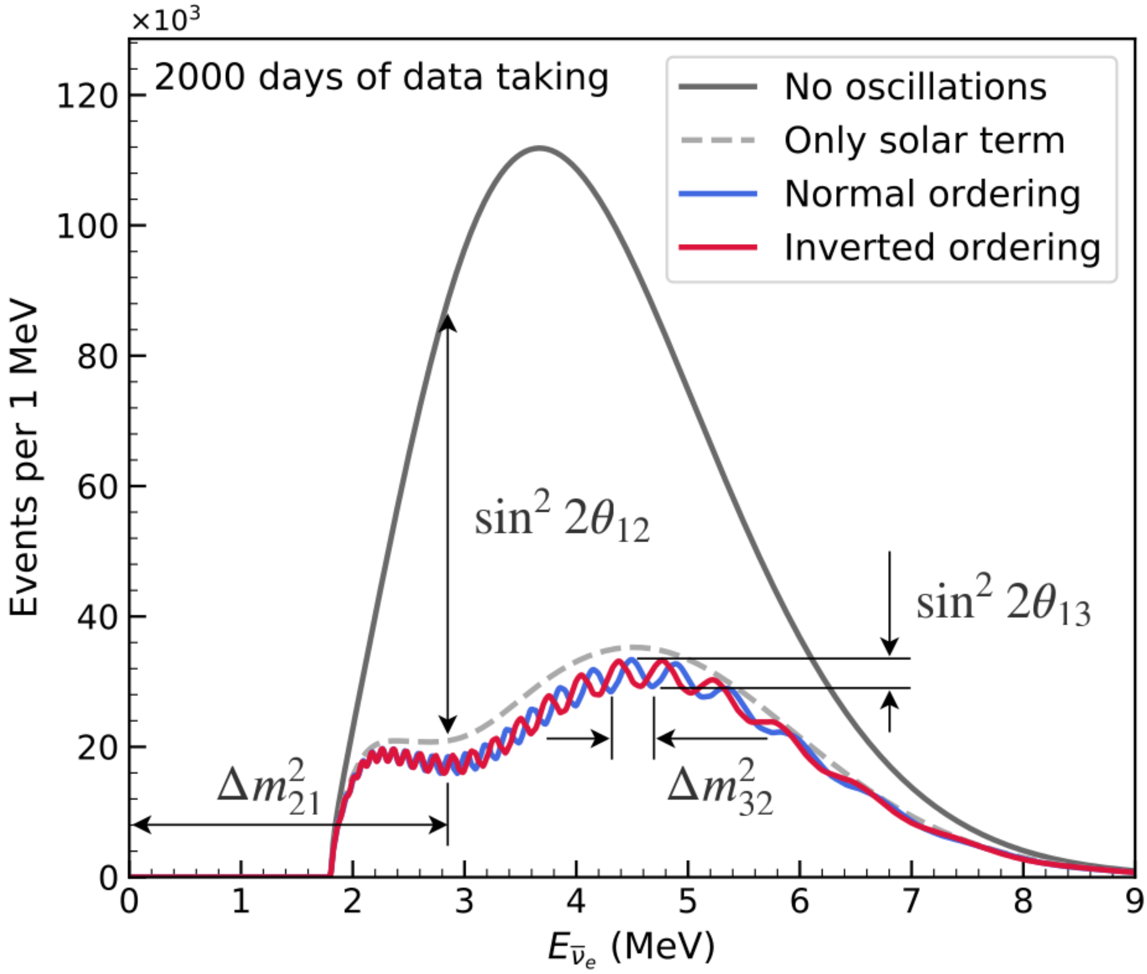

Figure 2: Expected spectrum

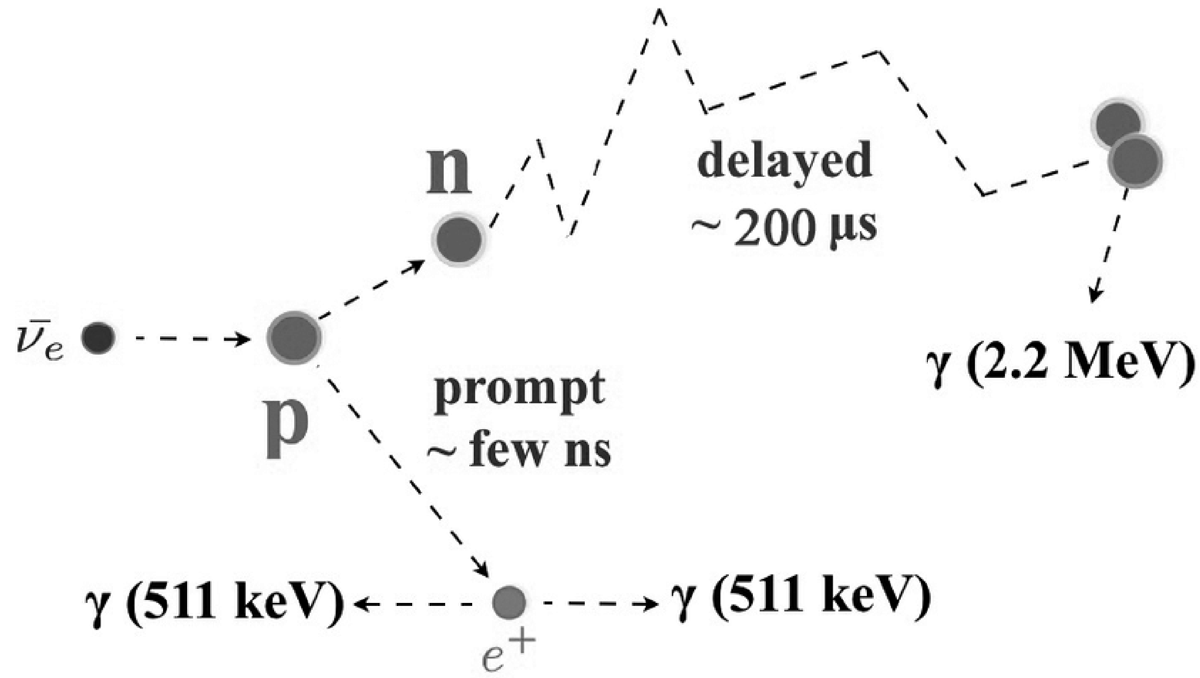

Figure 3: Antineutrino detection via IBD scheme.

These processes contribute to the "prompt" signal. The total visible energy of the prompt signal (E_{prompt}) is approximately:

$$E_{\text{prompt}} \approx E_{\bar{\nu}_e} - 0.782\,\text{MeV},$$

where the 0.782 MeV accounts for the neutron recoil energy (negligible, ~keV) and adjustments for the reaction kinematics.

The neutron from the IBD reaction initially carries $\sim$ 10–100 keV of kinetic energy and thermalizes via elastic scattering in the LS over $\sim$ 10–100 μs, losing energy until it reaches thermal energies (~ 0.025 eV). It then diffuses and is captured, predominantly on hydrogen (99% probability in undoped LS):

$$n + p \to d + \gamma \quad (E_\gamma = 2.223\,\text{MeV}),$$

or rarely on carbon ($\sim 1\%$):

$$n +^{12}\text{C} \to^{13}\text{C} + \gamma \quad (E_\gamma \approx 4.95\,\text{MeV}).$$

This "delayed" signal occurs with a mean capture time of $\sim 200\,\mu$s in JUNO's LS.

1.4 Detector design

The Jiangmen Underground Neutrino Observatory (JUNO) detector (Fig.4) is designed to detect neutrinos with high precision, using a large-scale setup with a central detector (CD), veto systems, and calibration systems, all housed in a shielded underground facility.

Centrad Detector

The CD is the heart of JUNO, featuring a large spherical acrylic vessel (35.4 m diameter) filled with 20,000 tons of liquid scintillator (LS), a special liquid that emits light when neutrinos interact with it. The vessel is made of acrylic panels bonded together and supported by a stainless steel structure to withstand the liquid's buoyancy. The LS is based on linear alkylbenzene (LAB) with additives to enhance light output, achieving high clarity (light travels $\geq 20\,\mathrm{m}$) and producing ~ 1100 photoelectrons per MeV for excellent energy resolution. The liquid is filled slowly with water to balance pressure, and circulation systems keep it pure and stable at $\sim 21°\mathrm{C}$.

The detector uses $\sim$ 17,600 20-inch photomultiplier tubes (PMTs) and $\sim$ 25,600 3-inch PMTs to capture the light from neutrino interactions, covering $\sim 78\%$ of the detector's surface. These PMTs convert light into electrical signals with high efficiency ($\sim 29\%$ detection efficiency) and low noise, ensuring accurate measurements. Electronics are housed in waterproof boxes underwater and on the surface, processing signals at high speed with minimal data loss. The system supports a data collection rate suitable for the experiment's needs over six years.

Veto Systems

- *Water Cherenkov Detector (WCD):* The CD is immersed in a 43.5 m wide, 44 m high pool filled with 35,000 tons of ultrapure water, acting as a shield against external radiation. It is equipped with 2,400 20-inch PMTs to detect muons (cosmic particles) with $\sim 99.8\%$ efficiency, keeping background noise low. Reflective materials in the pool enhance light collection.

- *Top Tracker (TT):* Above the pool, a system of plastic scintillator strips (reused from the OPERA experiment) covers part of the surface, tracking muons to further reduce background interference.

1.5 Background Challenges in Reactor Neutrino Experiments

Reactor neutrino experiments face significant challenges from various background sources that can mimic the characteristic delayed coincidence signature of inverse beta decay (IBD) reactions. The liquid scintillator (LS) detects IBD events by capturing the prompt positron signal ($E_{\text{prompt}} \approx E_\nu - 0.8\,\mathrm{MeV}$) and the delayed neutron capture signal ($E_\gamma \approx 2.2\,\mathrm{MeV}$ for hydrogen capture), with a time coincidence of $\sim 200\,\mu\mathrm{s}$ to suppress backgrounds. The inverse β-decay process provides a distinctive signature that enables background rejection, but several background sources can produce correlated events that mimic this IBD signature.

The technical challenges of JUNO include maintaining LS purity (attenuation length $> 20\,\mathrm{m}$ at 430 nm), achieving low background levels (e.g., $^{238}\mathrm{U}$ and $^{232}\mathrm{Th} < 10^{-17}\,\mathrm{g/g}$), and calibrating the detector's energy response to within 1%. The experiment's data acquisition system, with a trigger rate of $\sim 1\,\mathrm{kHz}$ and data rate of $\sim 50\,\mathrm{GB/s}$, employs advanced machine learning for event reconstruction and background rejection.

The two major background sources of JUNO are natural radioactivity and the products of cosmic muons. Natural radioactivity comes from all materials and the environment. Moreover, $^{13}\mathrm{C}(\alpha, n)^{16}\mathrm{O}$ reactions in the liquid scintillator result in correlated background events. Among these, cosmogenic backgrounds present some of the most challenging obstacles to precise neutrino measurements.

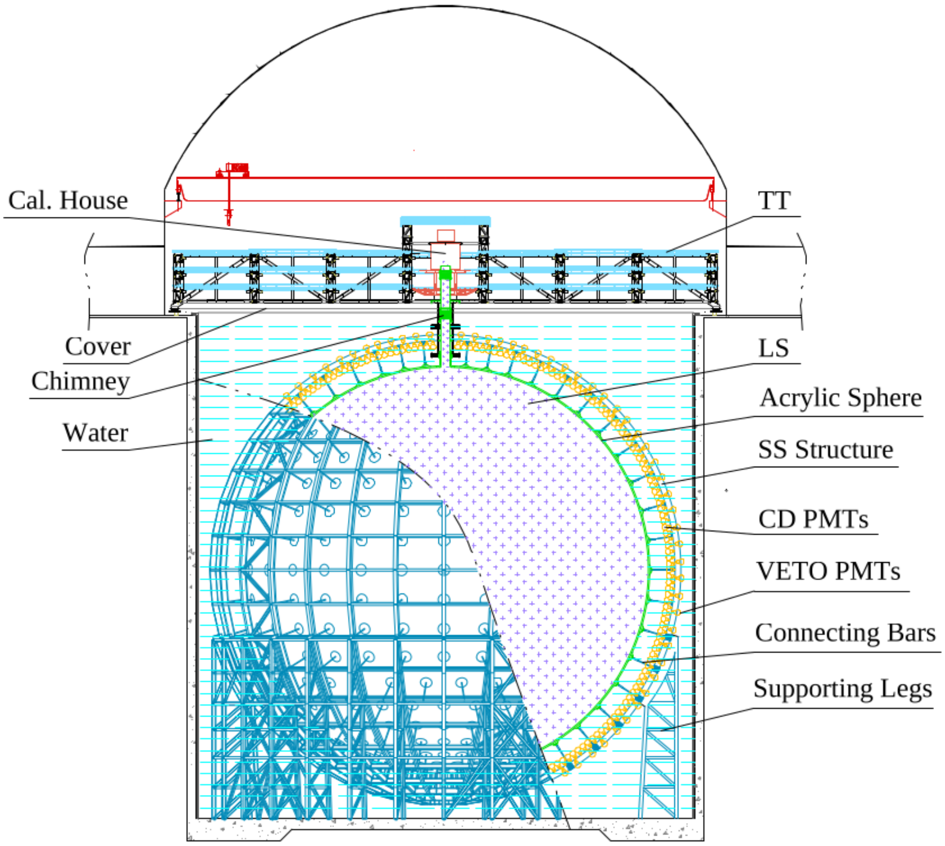

Figure 4: JUNO detector scheme.

1.6 Cosmogenic Backgrounds: The ^{8}He/^{9}Li Challenge

Cosmogenic backgrounds arise from the interaction of cosmic ray muons with the detector materials. Despite JUNO's substantial overburden of 693.35 m (1800 m.w.e.), the muon flux in the detector is $0.004\,\mathrm{s}^{-1}\mathrm{m}^{-2}$, still sufficient to produce significant backgrounds through various nuclear processes.

Among the most problematic cosmogenic isotopes are ^{8}He and ^{9}Li, which are produced when muons and their secondary particles interact with carbon nuclei in the liquid scintillator. Simulations were performed with GEANT4 to study ^{9}Li and ^{8}He production from muon interactions and their secondary shower particles in the liquid scintillator. Photonuclear reactions appear to dominate their production. The decays of these cosmogenic nuclei represent one of the largest irreducible backgrounds for reactor antineutrino experiments.

^{9}Li Background Characteristics

^{9}Li is particularly problematic due to its decay characteristics that closely mimic the IBD signal. With a half-life of 178 ms, ^{9}Li undergoes beta-minus decay to ^{9}Be*, which then emits a neutron and an alpha particle:

$$^{9}\mathrm{Li} \to {}^{9}\mathrm{Be}^{*} + e^{-} + \bar{\nu}_e$$

$$^{9}\mathrm{Be}^{*} \to {}^{8}\mathrm{Be} + n$$

$$^{8}\mathrm{Be} \to 2\alpha$$

This decay chain produces a prompt signal from the beta decay and a delayed signal from the neutron, creating a time-correlated event pair that can be mistaken for an IBD event. The energy spectrum and timing characteristics make ^{9}Li one of the most challenging backgrounds to reject.

^{8}He Background Properties

^{8}He, with its shorter half-life of 119 ms, also presents significant background challenges:

$$^{8}\mathrm{He} \to {}^{8}\mathrm{Li} + e^{-} + \bar{\nu}_e + n$$

Similar to ^{9}Li, the ^{8}He decay produces correlated prompt and delayed signals that can mimic IBD signatures, making it another critical background component that requires careful study and rejection strategies.

2 Problems

2.1 Cutting volume determination.

In experiment muon tracks are always reconstructed with some uncertainty (Fig.5). Because of that inaccurate muon track reconstruction it's important to understand how cutting volume related to reconstructed track affects amount of isotopes created by real track.

To approach this problem the first thing to do is to make a histogram (or map) of cutting detector volume efficiency. Let R be the distance from reconstructed track to center of detector and r – simulated to reconstructed track distance. Efficiency in this case is defined as ratio of intersection volume of cylinder with radius r and axis-to-detector

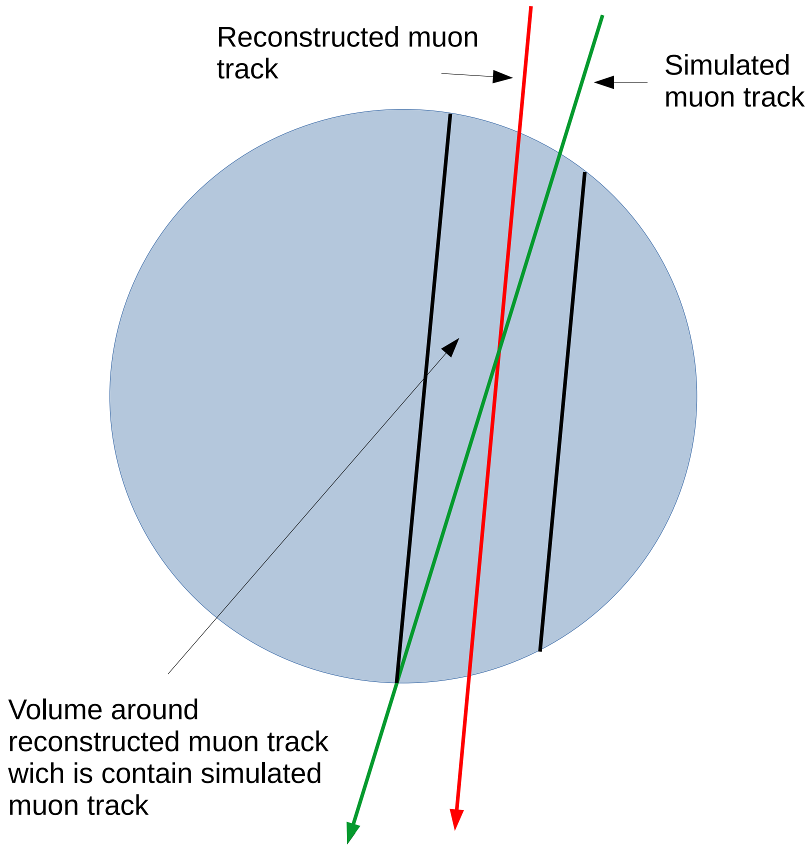

Figure 5: Uncertainty of muon track reconstruction.

center distance R to volume of central detector with radius $a = 17.7$ m. This histogram will be commonly used in the following tasks.

So, one has to find intersection volumes of cylinder with given R and r and central detector with radius a. The analytical approach seems difficult, thus numerical methods were used.

The idea behind used method is to fill space with points, count amount of them that fall into the intersection of cylinder and CD, then calculate the ratio of these to all the dots. Given known volume of spanned space it gets trivial to find the volume of intersection. Monte-Carlo method is standard for such tasks, but it takes too much time for program to be executed.

Homogeneous grid spanning cube with edge length $L = 40$ m instead of using Monte-Carlo was used in this work. The x-grid and y-grid arrays are created and for each pair (x, y) number of z points within the CD are calculated. Then for different fixed R and r if (x, y) belongs to cylinder and CD the amount of z-points gets summed. Such a way of calculation is used in other following tasks. Unforunately for given accuracy execution time of program is quite long. To reduce run time OpenMP parallel programming interface was used.

The resulting histogram is shown on Fig. 6

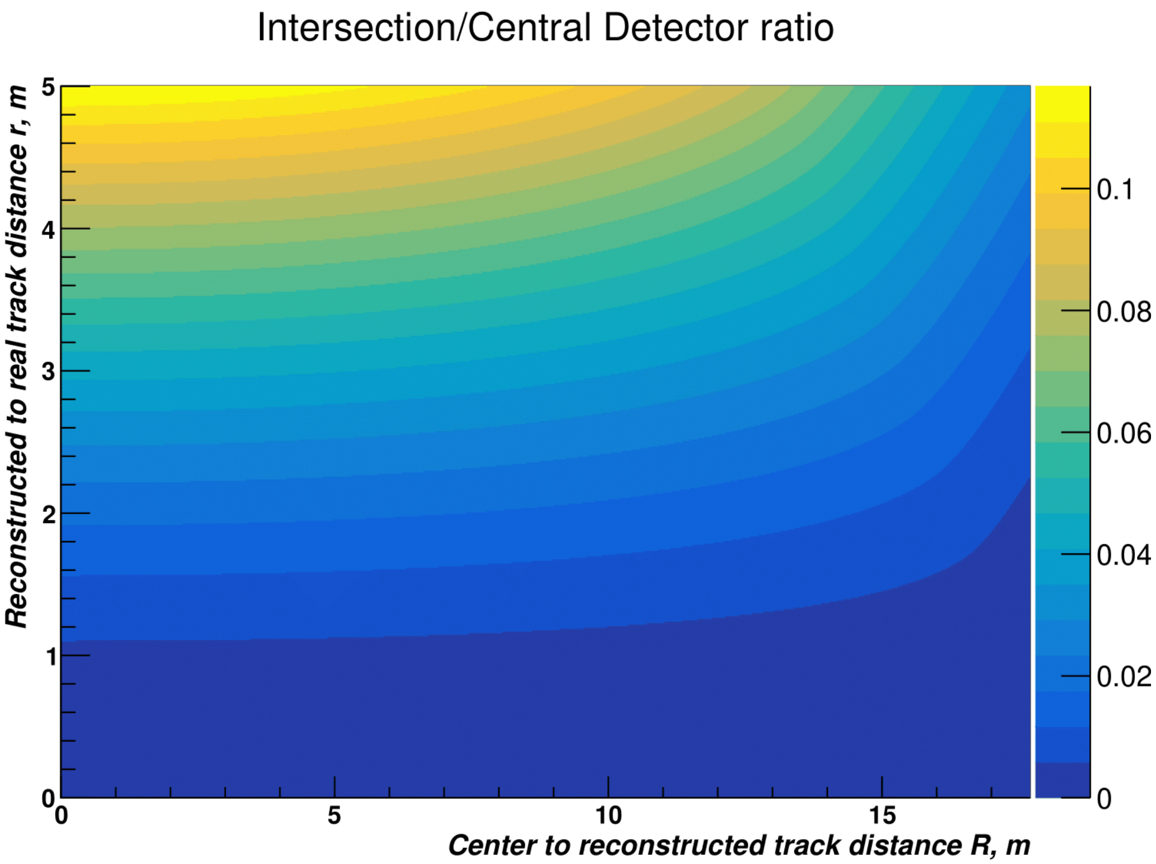

Figure 6: Histogram representing V_{int}/V_{CD}, where V_{int} is intersection volume of cylinder with radius r and axis-to-CD distance R and CD volume.

2.2 Isotopes distribution.

In order to efficiently get rid of isotope-filled volume it's essential to know their distribution around muon track. Bunch of muon tracks was simulated and pushed through the detector in Geant4 framework. Muons interacted with scintillator creating a number of radioactive isotopes ^{8}He/^{9}Li. Using this simulated data, the number of isotopes with respect to distance to corresponding muon track was determined.

As it can be seen from obtained histogram (Fig.7), number of isotopes declines very rapidly for distances more than 0.4 m and is almost zero at 5 m. Taking this into account, it will be considered that there are no isotopes at distances exceeding 5 meters.

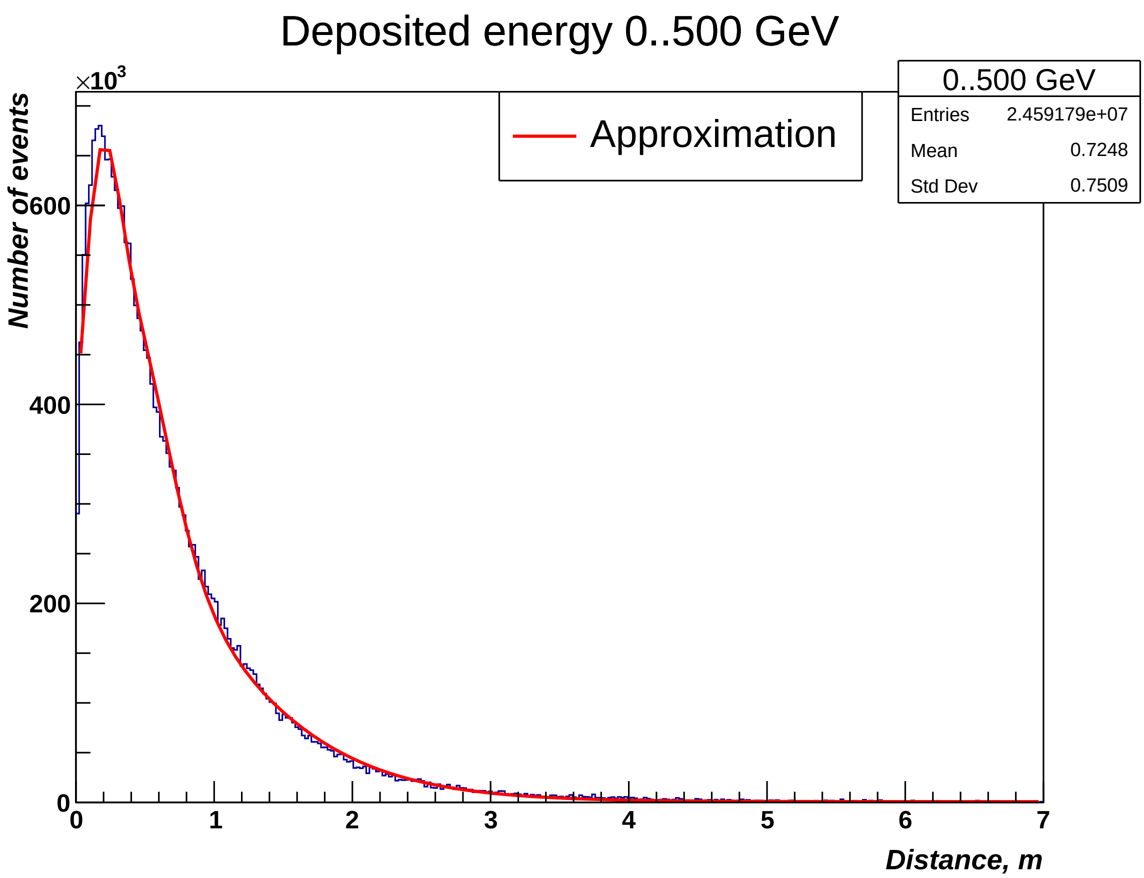

Figure 7: Isotopes distribution in deposited energy range 0 to 500 GeV around muon track.

It's also important to get fitting function for this distribution. This functinon will be used further. Approximation was performed using following function:

$$f(x) = p_1 + p_2 x \exp(p_3 - p_4 x) + p_5 x \exp(p_6 - p_7 x^2) + p_8 \exp(p_9 - p_{10} x^3)$$

Table 1: Approximation function parameters' values

p_1	p_2	p_3	p_4	p_5	p_6	p_7	p_8	p_9	p_{10}
722.7	4.919	12.438	2.0214	3.094	12.9199	4.010	3.678	11.510	32.97

This approximation is not very accurate, but it's enough for purposes of the problem.

2.3 Background suppression efficiency.

The next thing to do is evaluate mean efficincies of volume and isotopes cutting for cylinder with fixed radius. Volume cutting efficiency ε_V is fraction of whole central detector volume after cylindrical region is cut out. Isotopes cutting efficiency ε_{iso} is ratio of isotopes withing cylinder volume to all the isotopes created by muon.

$$\varepsilon_V = 1 - \frac{V_{cyl}}{V_{CD}}$$

$$\varepsilon_{iso} = \frac{N_{iso}^{in}}{N_{iso}^{all}}$$

Mean volume efficiency is weighted: cylinder volumes correspoding to different R values are included to the sum with different coefficients. Muon flux is almost homogeneous so the number of tracks going through detector element is in direct ratio with it's area. Hence coefficient $k(R)$ for cylinder with axis to CD center distance R is ratio of corona circular with smaller radius R and width dR to area of circle with radius a.

$$\langle \tilde{\varepsilon}_V(d) \rangle = \sum_{i=0}^{N} k(R_i) \tilde{\varepsilon}_V(R_i, d)$$

$$k(R_i) = \frac{\pi \left[(R_i + \Delta R)^2 - R_i^2 \right]}{\pi a^2} = \frac{2R_i \Delta R + (\Delta R)^2}{a^2}$$

$$\langle \varepsilon_V(d) \rangle = 1 - \langle \tilde{\varepsilon}_V(d) \rangle$$

Mean isotopes efficiency is calculated as

$$\langle \varepsilon_{iso}(d) \rangle = \frac{1}{N} \sum_{i=0}^{N} \varepsilon_{iso}(R_i, d)$$

ε_{iso} is found using the same method as in first task. There is a grid that spans the space. Considering that distribution is axially symmetric the isotopes concentration is calculated for each point of grid that belongs to intersection of cylinder and CD. By summing these concentration values divided by number of all points in the grid and multiplied by space volume we get the number of isotopes in cylinder. Also, the whole number of isotopes in central detector is found. Then efficiency of isotope embracing is just ratio of "in" to "all".

2.4 Impact of track reconstruction uncertainty on background suppression.

As mentioned earlier, reconstructed muon tracks are shifted from real ones. This means that isotopes distribution is known with respect to real track. Next task will be to find out the fraction of isotopes embraced by cutting volume cylinder depending on it's distance to simulated (real) track. We take cylinder's radius equal to the maximum distance to real track.

Solving this problem is still in progress.

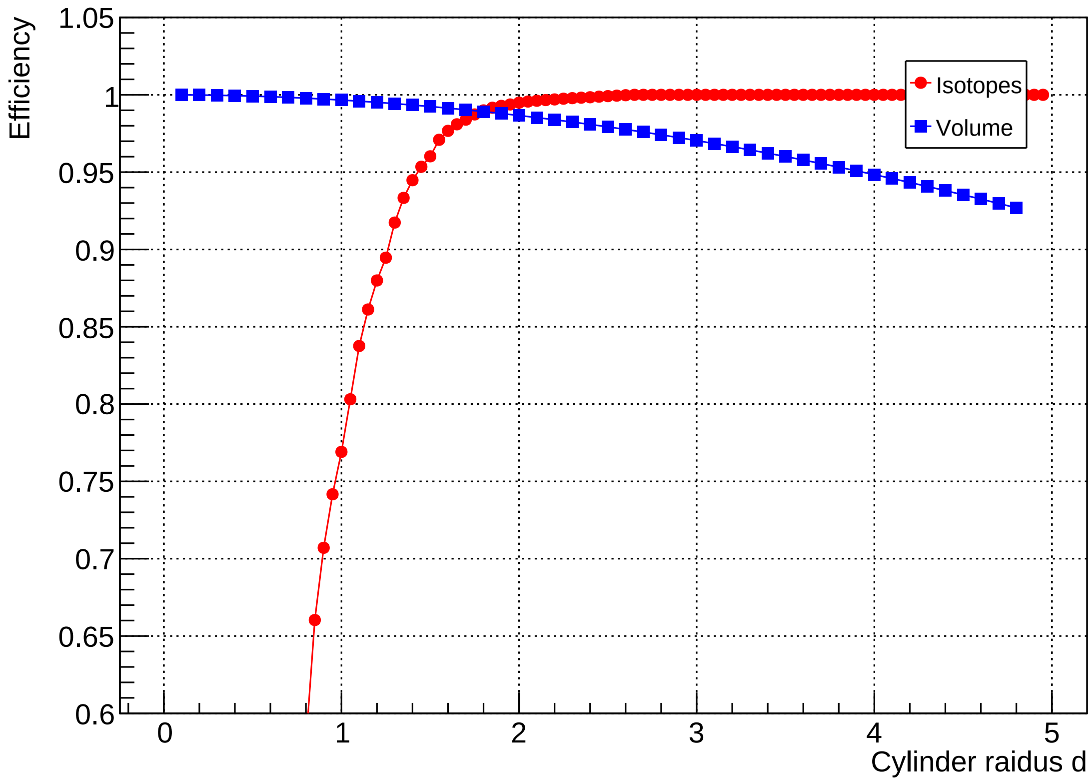

Figure 8: Efficiencies

3 Conclusion

This work studied the ^{8}He/^{9}Li background problem in the JUNO experiment using computer simulations and numerical calculations. The main results are:

- **Isotope Distribution:** Most isotopes are created very close to muon tracks—within 0.4 m. Almost no isotopes are found at distances more than 5 m from the track. This is important for deciding how big the cutting volume should be.
- **Efficiency Calculations:** A method was created to calculate how much detector volume is lost when cutting cylindrical regions around muon tracks, and how many background isotopes are removed. This helps to find the best balance between keeping detector volume and removing background.
- **Computer Methods:** The calculations were made faster using parallel computing with OpenMP because the volume intersection problems take a long time to solve.
- **Practical Results:** The efficiency curves can be used directly in JUNO data analysis to decide the best strategy for removing muon-related backgrounds.

The results show that it is possible to remove most of the cosmogenic background without losing too much detector volume. Since isotopes are created mostly very close to muon tracks, cutting cylindrical volumes around these tracks can remove a lot of background while keeping most of the detector available for neutrino detection.

Future Work There are several things that should be done next:

- **Finish Problem 4:** Complete the analysis of how track reconstruction errors affect the cutting efficiency.
- **Find Best Parameters:** Use optimization methods to find the best cutting parameters that give good background removal with minimal volume loss.
- **Check with Real Data:** Compare the simulation results with actual JUNO data when it becomes available.

4 References

- JUNO Collaboration. JUNO Physics and Detector, arXiv:1507.05613
- JUNO Collaboration. JUNO Conceptual Design Report, arXiv:1508.07166
- An, F. P., et al. (JUNO Collaboration). J. Phys. G: Nucl. Part. Phys., 43, 030401
- Abusleme, A., et al. (JUNO Collaboration). Eur. Phys. J. C, 81, 1030